

pubs.acs.org/JACS Article

Acid-Dependent Charge Transport in a Solution-Processed 2D Conductive Metal-Organic Framework

Geunchan Park, Monique C. Demuth, Christopher H. Hendon,* and Sarah S. Park*



Cite This: https://doi.org/10.1021/jacs.4c02326



Read Online

ACCESS

Metrics & More

Article Recommendations

Supporting Information

ABSTRACT: The development of conductive metal-organic frameworks (MOFs) presents a unique challenge in materials chemistry because it is unclear how to dope them. Here, we demonstrate that the inclusion of pendant amines on hexahydroxytriphenylene linkages results in two-dimensional (2D) polycrystalline frameworks Cu₃(HHTATP)₂, isostructural to its Cu₃(HHTP)₂ parent, and exhibits the highest electrical conductivity of 1.21 S/cm among 2D MOFs featuring CuO₄ metal nodes. Moreover, the bulk material can be treated with acid, resulting in a protonation-dependent increase in the conductivity. By spin-coating the acidic solution, we fabricated large-area thin films and collectively demonstrated an intuitive route to solution-processable, dopable, conductive MOFs.



INTRODUCTION

Two-dimensional (2D) electrically conductive metal-organic frameworks (MOFs) are a subset of porous materials that are emerging as useful materials in electrocatalysis, ^{1,2} energy storage, ^{3–5} sensing, ⁶ and electronic devices ⁷ due to their outstanding charge-transport properties paired with their high porosity. ⁸ Yet, these materials face significant challenges in establishing design strategies to control both electrical and chemical properties, including limited methods to dope them. ⁹ The development of MOFs with synthetically intuitive handles to control the Fermi level is a major milestone.

Toward this effort, the champion materials comprise of planar, tritopic ligands, and studies have probed both the effect of substituting ligating heteroatoms (i.e., substituting S-, O-, and NH- of)¹⁰⁻¹² and their interplay with ligated metal (i.e., analogues made from Co, Ni, Cu, Fe, Zn, Pd, Pt, etc.).¹³⁻¹⁷ Previous studies have emphasized the importance of introducing electron-rich chelating motifs (-NH₂, -SH) to organic linkers to enhance orbital overlaps between the metal cations and linkers.^{8,18,19} There remains burgeoning interest in designing new tritopic linkers with dissimilar conjugated cores^{20,21} and points to a central design principle: in-plane metal ligand covalency dictates bulk electrical conductivity. Thus, beyond substitution of metal and/or heteroatom, there is value in exploring other chemical handles that affects their interfacial chemistry.²²

In addition to their electrical properties, the facile processing of 2D MOFs into thin films is crucial for their application in electronic devices. To achieve this, various fabrication techniques, including chemical vapor deposition, layer-by-layer, and microfluidic synthesis, have been employed to craft high-quality thin films. In contrast, widely used solvothermal methods for synthesizing MOFs result in reduced solution processability due to limited control over crystallite

size.²⁷ Hence, the development of design strategies for achieving processable bulk materials is essential to ensure the suitability of 2D MOFs for device-friendly applications.

Considering both the compositional and synthetic studies, the resultant electrical conductivity of 2D MOFs is largely dictated by stacking faults, adatoms, and vacancies, 9,28,29 and only a limited amount of attention has been devoted to the control of electrical conductivity and chemical properties through modifications during and after the synthesis. 10,30 Here, we present a general approach to providing a chemical handle for doping: the inclusion of electron-donating, Brønsted-basic pendant aromatic amines on otherwise planar π -conjugated linkers (Figure 1b). Like other aminated multitopic linkers, amino-functionalization should result in maintained 2D crystal connectivity while providing a pH-dependent chemical handle to modify the π -electron energy. 31

Motivated by this, we developed a Cu-based MOF composed of the HHTATP linker (HHTATP = 2,3,6,7,10,11-hexahydroxy-1,5,9-triaminotriphenylene). Building upon a previous study that suggested that linker antiaromaticity is a predictor of bulk electrical conductivity, we first sought to determine whether amination of the HHTP linker was expected to negatively impact the linker aromaticity.³² Using the NICS-xy formalism, aromaticity was probed by sampling the NMR shielding of a dummy atom located 1.7 Å above the ring faces (Figure S3). Both HHTP

Received: February 15, 2024 Revised: April 2, 2024 Accepted: April 3, 2024



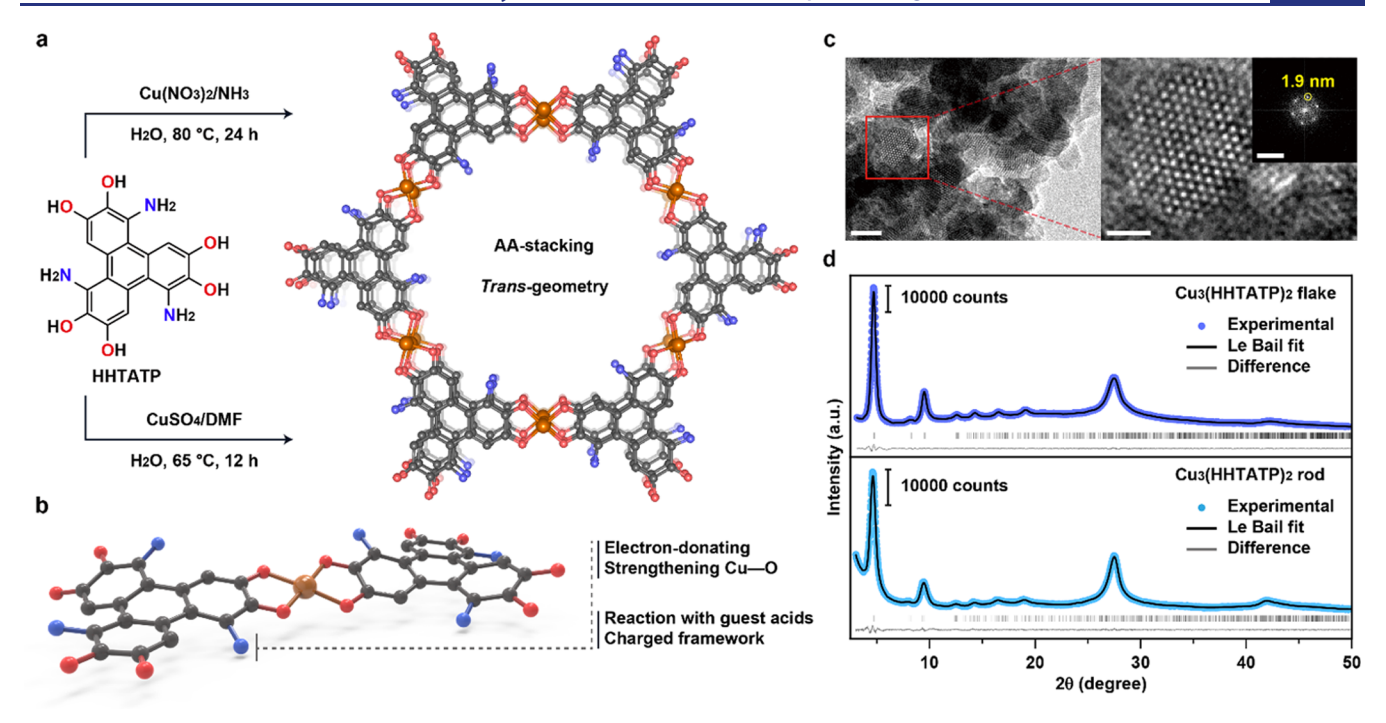


Figure 1. (a) Chemical structure of HHTATP and schematic of the conductive 2D MOF. Hydrogens are omitted for clarity. (b) Molecular approach toward conductive and porous 2D scaffolds. (c) TEM images of $Cu_3(HHTATP)_2$ nanoflakes. Left scale bar: 25 nm; right scale bar: 10 nm (inset: FFT image of the micrograph with scale bar: 1 nm⁻¹). (d) PXRD patterns and corresponding Le Bail fittings for the $Cu_3(HHTATP)_2$ nanoflake (λ : 1.5406 Å) and the nanorod (λ : 1.5309 Å).

and HHTATP show comparable antiaromaticity, suggesting that the aromaticity of the rings is not greatly affected by the amino substituents and should yield similarly conductive frameworks made therefrom. However, the HHTATP linker has explicit $-NH_2$, which can be used as allosteric handles to affect the aromaticity.

■ RESULTS AND DISCUSSION

Cu₃(HHTATP)₂ was synthesized via a solvothermal reaction involving HHTATP and a copper(II) source (either sulfate pentahydrate (CuSO₄·SH₂O) or nitrate trihydrate (Cu(NO₃)₂·3H₂O)). The reactions were carried out in air using *N,N*-dimethylformamide and aqueous NH₃ as crystal growth modulators (Figure 1a). Both copper sources produce dark powders, with the sulfate precursor yielding nanorods and the nitrate precursor yielding stacked nanoflakes, as measured by scanning electron microscopy (Figure S4). Powder X-ray diffraction (PXRD) patterns of the two nanocrystal morphologies (Figures 1d and S5) reveal crystallinity with sets of peaks. Both (100) and (200) reflections at $2\theta = 4.7$ and 9.5° , respectively, are positioned similarly to the previously reported Cu₃(HHTP)₂ and Ni₃(HITP)₂.

The Fourier-transform infrared (FTIR) spectrum of both free linker, HHTATP, and Cu₃(HHTATP)₂ (Figure S6) revealed aromatic amine C–N stretching at 1296 cm⁻¹, with both rod and flake crystals exhibiting an identical pattern, indicating the retention of amines during synthesis. To ascertain the oxidation states of nitrogen, X-ray photoelectron spectroscopy (XPS) data was collected (Figure S7), revealing a broad N(1s) signal around 399.5 eV. This suggests slight variations in oxidation states due to electronic interactions with the aromatic centers.³⁴ This feature is more pronounced in the near-edge X-ray absorption fine structure (NEXAFS) pattern of nitrogen K-edge (Figure 2a), displaying peaks at 399.4 eV

(1s $\to \pi_{\rm N-C}$) and 400.7 eV (1s $\to \pi_{\rm C-C}$), indicating the participation of lone pairs in p-orbitals of amine groups in a π -conjugated system.³⁵

Although the free linker is achiral, its incorporation into the material can result in various ligand configurations, some chiral and some achiral (Figure S3). Density functional theory

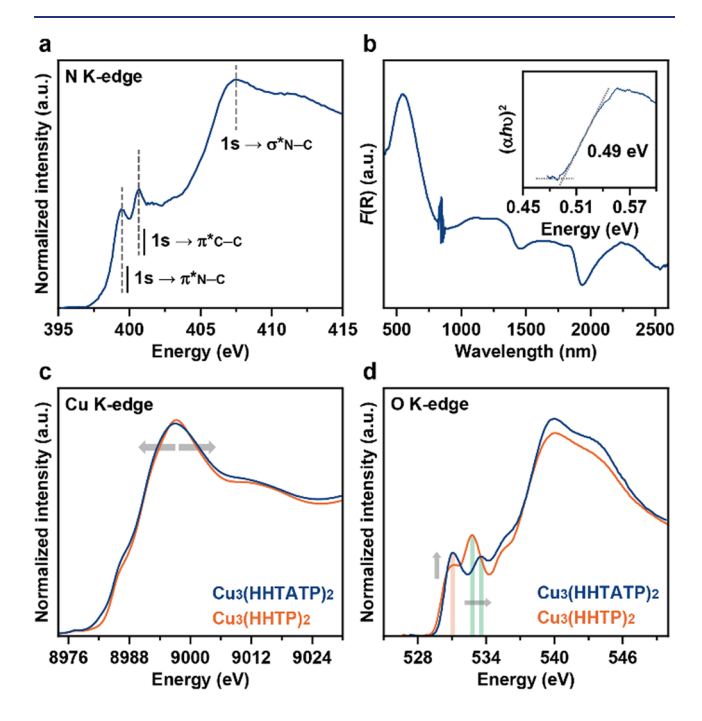


Figure 2. (a) N K-edge soft XAS and (b) DRUV—vis spectra of $\text{Cu}_3(\text{HHTATP})_2$ (inset: Tauc plot). (c) Cu K-edge XANES and (d) O K-edge soft XAS spectra.

(DFT) calculations were performed on four candidate model structures (Supporting Information (SI)), and their relative energies, predicted PXRD patterns, and electronic properties were compared. DFT predicts that the MOF is an out-of-plane (i.e., π -conducting) metal, Figure 3, and is anticipated to have a

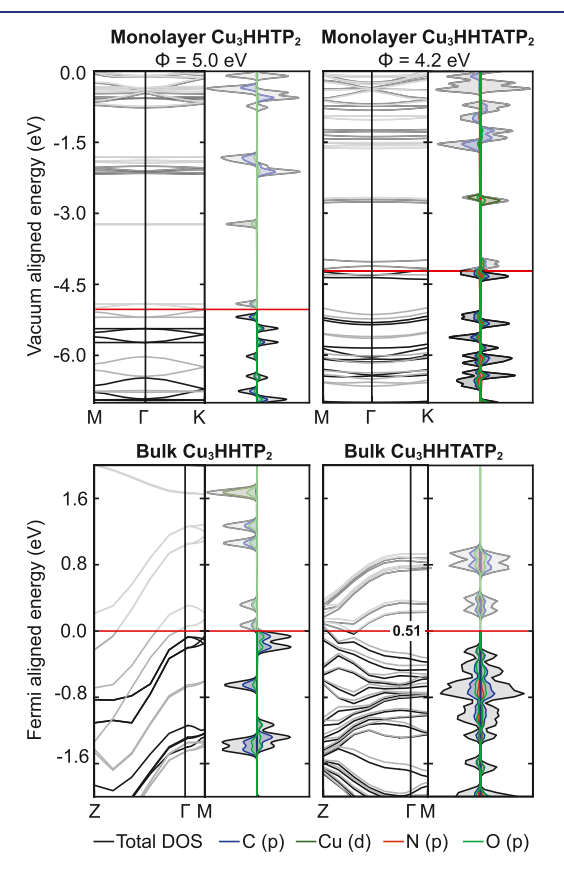


Figure 3. Band structures for monolayer and bulk Cu_3HHTP_2 and $Cu_3HHTATP_2$. Monolayer HHTATP has a smaller workfunction associated with amination of the triphenylene core. The bulk structure features out-of-plane metallicity in the eclipsed configuration and results in a marginal increase in the in-plane electronic gap, accessible upon stacking disorder. The density of states is presented at the *γ*-point only.

slightly wavy structure (Figure S8) associated with the propensity for Cu to distort and oxidation of the linker. Further, the lowest energy amine configuration was isolated, together predicting a near-eclipsed (AA) stacking. Other configurations exhibited similar electronic properties independent of ligand orientation. This excellent agreement with experiment bolsters the Le Bail fitting for both the nanoflake and the nanorod (Figure 1d and Table S1).

Cryogenic electron microscopy (Figure S9) reveals an interlayer stacking structure with slightly diffusive arcs, approximately 0.32 nm in real space, representing the interlayer distance of $\text{Cu}_3(\text{HHTATP})_2$. This value aligns with the $d_{(002)}=0.324$ nm in the PXRD pattern and the interlayer spacing predicted from DFT (0.334 nm). Additionally, the transmission electron microscopy (TEM) images depict the expected honeycomb lattices viewed along the [001] direction (Figures 1c and S10). The corresponding Fourier transform reveals a lattice parameter of 1.9 nm, matching with the $d_{(100)}=1.88$ nm in the PXRD, and the DFT result (1.87 nm). The structure's porosity was further explored through N₂

adsorption isotherm at 77 K (Figure S11 and Table S2), displaying Brunauer–Emmett–Teller (BET) surface areas of 239 $\rm m^2/g$ for the rod and 302 $\rm m^2/g$ for the flake, with the pore diameter derived from nonlocal DFT being 1.4 nm, with a theoretical maximum specific surface area of 956 $\rm m^2/g$. While the pore aperture is in good agreement with the theoretical pore size (1.43 nm), the reduced accessible surface area is likely due to stacking faults and pore occlusion. Nonetheless, the experimental values are in line with those of other isostructural 2D MOFs. 16,36

To gain insights into the electronic structure, we invoked Xray absorption near-edge spectroscopy (XANES) to observe the copper K-edge for both MOFs (Figure 2c). These experiments revealed a slightly broader rising edge around 8.997 keV, indicating greater delocalization of the outer electronic shells of Cu^{2+} in $\text{Cu}_3(\text{HHTATP})_2$. 37,38 Concurrently, NEXAFS spectra of oxygen K-edge (Figure 2d) were obtained, featuring an intensified O 1s \rightarrow Cu 3d peak at 531.1 eV, signifying enhanced covalency in the Cu-O bond. 39,40 This is also underpinned by the more thermally robust structure of Cu₃(HHTATP)₂ compared to that of Cu₃(HHTP)₂ (Figure S12). Meanwhile, a decreased, blueshifted 1s $\rightarrow \pi_{C-O}$ peak at 533.6 eV suggests that the ligandcentered lowest unoccupied molecular orbital (LUMO) level is above that of Cu₃(HHTP)₂.³⁹ DFT electronic band structure calculations of the monolayer align with this measurement (Figure 3), implying that the narrower optical gap is a result of destabilized d-orbitals in a Cu^{2+} with a π -character rather than the effects of LUMO states in the organic linkers.

In contrast to the $\text{Cu}_3(\text{HHTP})_2$, a diffuse-reflectance UV–vis (DRUV–vis) spectrum of $\text{Cu}_3(\text{HHTATP})_2$ (Figure 2b) exhibits multiple broad absorptions at ~1200, ~1700, and ~2200 nm⁴¹ when represented in Tauc coordinates for direct allowed transitions, as expected from the DFT band structure for the in-plane electronic gap (Figure 3). The DFT-computed in-plane gap from the bulk calculation (0.51 eV) matches closely with the experimental value (0.49 eV, Figure 2b).⁴¹

The Cu₃(HHTATP)₂ crystallites are readily dispersed in various solvents, forming stable suspensions persisting beyond 1 week, exceeding Cu₃(HHTP)₂ suspensions which tend to reaggregate (Figures S13 and S14). Treating the Cu₃(HHTATP)₂ suspension in DMSO with trifluoroacetic acid (TFA) results in a homogeneous dark blue solution (Figure S15), a phenomenon unprecedented in any electrically conductive 2D MOFs to our knowledge. To investigate the relationship between solvation and the amine group, NEXAFS for the nitrogen K-edge (Figure S16) was conducted. The spectrum of the reprecipitates exhibits a 1s $\rightarrow \sigma^*_{N-H}$ peak at 401.6 eV, absent in the pristine material.⁴² Additionally, this signal gradually diminishes when the reprecipitate is washed with reagent alcohol or Et₃N/THF solution, indicating that the solvation process involves protonation of the amine groups. The dissolving nature without a structural deformation was initially confirmed by a PXRD measurement of reprecipitates from the solutions (Figure S17), retaining the (100), (200), and (002) reflections. The slightly amorphized PXRD profile, manifesting as a broad hump over $2\theta = 15-25^{\circ}$, may result from the rapid recrystallization process over ethyl acetate, causing disordered stacking and resembling the acid-mediated exfoliation reported in covalent-organic frameworks. 43,44

With the framework suspended, we fabricated large-area thin films of $\text{Cu}_3(\text{HHTATP})_2$ through spin-coating the viscous DMSO/TFA solution (Figure 4a). To analyze the quality of

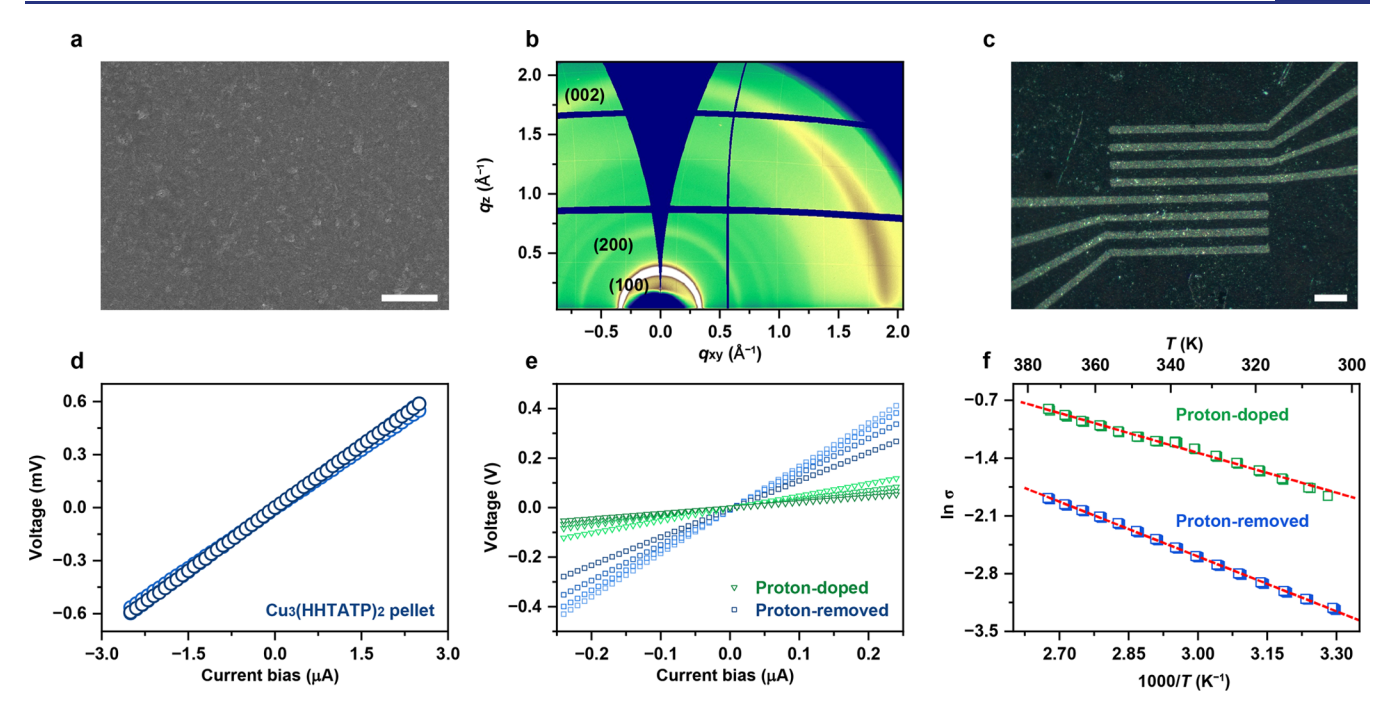


Figure 4. (a) SEM image (scale bar: $2 \mu m$) and (b) a two-dimensional GIWAXS pattern of the $Cu_3(HHTATP)_2$ proton-doped thin film. (c) Optical microscopic image of the thin film device (scale bar: $100 \mu m$). 4-Point probe resistance measurements of (d) the $Cu_3(HHTATP)_2$ rod pellet and (e) the film devices. (f) Plots of $\ln \sigma$ versus 1/T well fit to the thermally activated charge transport.

the film, atomic force microscopy (AFM) was performed on a film scratched by a razorblade (Figure S18), showing a thickness of 85 nm with a 19.6 nm root-mean-square roughness of the total area. For further analysis, grazingincidence wide-angle X-ray scattering (GIWAXS) measurement was performed on these films (Figures 4b and S19), displaying ring signals at $q = 0.34 \text{ Å}^{-1}$ and $q = 0.67 \text{ Å}^{-1}$, corresponding to the (100) and (200) reflections found in the PXRD pattern of the pristine MOF. Signals around q = 1.93Å-1 aligned with the (002) reflection and were more pronounced along the in-plane direction than out-of-plane, suggesting a slight edge-on orientation of the crystallites. Furthermore, an in-plane diffraction profile of the film washed with aprotic solvents (proton-doped) exhibited a shift of the (002) reflection to a lower q value compared to the film washed with a basic solution, 0.1 M Et₃N/THF (protonremoved, Figure S20), and the pristine powder, indicating a widened stacking distance in the protonated framework.

To assess the electrical properties, we conducted a fourprobe resistivity measurement on both a pressed pellet and representative spin-coated films. While the bulk electrical conductivity of the $Cu_3(HHTATP)_2$ flake showed 3.9 (± 0.4) \times 10⁻² S/cm (Figure S21), which is comparable with the $Cu_3(HHTP)_2$, the $Cu_3(HHTATP)_2$ rod exceeded that of $Cu_3(HHTP)_2$ by 18-54 times, $^{3,35,45-48}$ reaching as high as 1.21 (± 0.01) S/cm at room temperature (RT) (Figure 4d). This conductivity stands as the highest among pellets of 2D MOFs featuring CuO₄ metal nodes (Tables S3 and S4). To identify the major charge carrier in the framework, four-probe measurements were performed on the proton-doped and removed films (Figure 4c,e). The proton-doped films exhibited almost 5-fold higher conductivity of 0.12 (\pm 0.04) S/cm than the proton-removed films of 2.5 (± 0.5) \times 10⁻² S/cm at RT, suggesting that charge transport in Cu₃(HHTATP)₂ predominantly occurs through hole conduction rather than electrons. The hypothesis further bolstered the NICS-xy scans of the

linker in various protonation states. Aligning with our hypothesis that conductivity was proportional to the extent of linker antiaromaticity, ³² our calculations presented in Figure S3 suggest that protonation marginally increases antiaromaticity.

Variable-temperature conductivity measurements in the high-temperature range (Figure 4f) reveal thermally activated charge-hopping, with a lower activation energy $E_{\rm a}=138~{\rm meV}$ for the proton-doped film compared to the proton-removed film ($E_{\rm a}=191~{\rm meV}$). These activation energies imply that thermally activated carriers have a weaker impact on charge transportation in the proton-doped film, while phonon scattering operates vice versa. Despite nanoscale responses in current to external electrical fields in the transistors (Figure S22), the transfer curves indicate a slight amplification of drain currents along the negative gate voltage, suggesting p-type conduction in Cu₃(HHTATP)₂, possibly due to the electron-enriched framework facilitated by pendant amines in the linker. 10,49

CONCLUSIONS

In summary, our study demonstrates that modifying non-coordinating functional groups can alter the electronic structure of a conjugated π -system within the framework, influencing its chemical properties with guest species. The introduction of amine groups resulted in enhanced charge delocalization and inevitably resulted in highly conductive samples as measured using a 4-point probe method. The addition of the amines resulted in the material dispersed in polar solvents with acid, enabling the straightforward fabrication of large-area thin films through a simple spin-coating process. The same conditions lead to the formation of a tunable p-type conductor and generally offer valuable insights for developing synthesis-friendly strategies to tailor electrical and chemical properties in 2D MOFs. Moreover, we anticipate

that functionalizations into other groups (electron-withdrawing, redox-active, etc.,) will yield novel framework properties and enable access to readily doped MOFs.

ASSOCIATED CONTENT

5 Supporting Information

The Supporting Information is available free of charge at https://pubs.acs.org/doi/10.1021/jacs.4c02326.

Detailed experimental and computational methods; NMR; scanning electron microscopy (SEM) images; powder X-ray diffraction data; thermogravimetric analysis (TGA); and N₂ adsorption isotherms (PDF)

AUTHOR INFORMATION

Corresponding Authors

Christopher H. Hendon — Department of Chemistry and Biochemistry, University of Oregon, Eugene, Oregon 97403, United States; ⊚ orcid.org/0000-0002-7132-768X; Email: chendon@uoregon.edu

Sarah S. Park — Department of Chemistry, Pohang University of Science and Technology (POSTECH), Pohang 37673, Republic of Korea; Institute for Convergence Research and Education in Advanced Technology (I-CREATE), Yonsei University, Seoul 03722, Republic of Korea; orcid.org/0000-0002-8770-6094; Email: sarahpark@postech.ac.kr

Authors

Geunchan Park – Department of Chemistry, Pohang University of Science and Technology (POSTECH), Pohang 37673, Republic of Korea

Monique C. Demuth – Department of Chemistry and Biochemistry, University of Oregon, Eugene, Oregon 97403, United States

Complete contact information is available at: https://pubs.acs.org/10.1021/jacs.4c02326

Notes

The authors declare no competing financial interest.

ACKNOWLEDGMENTS

The X-ray diffraction was performed at 9B beamline, the wideangle X-ray scattering at 3C beamline, the X-ray absorption at 10A2, 8C, and 4D beamlines, X-ray photoelectron spectroscopy at 10A2 beamline of the Pohang Accelerator Laboratory (PAL), Korea. The SEM was performed at the National Institute for Nanomaterials Technology (NINT) in Pohang, Korea. Experimental aspects of this paper are supported by National Research Foundation of Korea (NRF) grants funded by the Korean government (NRF-RS-2023-00212896 and NRF-2020R1A5A1019141). Computational aspects of this paper are supported by the National Science Foundation through the Division of Materials Research under grant no. DMR-1956403 and the Camille and Henry Dreyfus Foundation. This work used Expanse at SDSC through allocation CHE160003 from the Advanced Cyberinfrastructure Coordination Ecosystem: Services and Support (ACCESS) program, which is supported by the National Science Foundation grants #2138259, #2138286, #2138307, #2137603, and #2138296. We thank Prof. Keehoon Kang for helpful discussions on FET device fabrication, Dr. Youngyong Kim for helpful discussions on GIWAXS experiments, Yurim Hong for TEM measurements, and Hyesoo Kim, Myeonggeun

Choe, Kwangjin Song, and Yelim Son for their assistance with the conductivity, DRUV—vis, TGA, and AFM measurements.

REFERENCES

- (1) Kim, M.; Yi, J.; Park, S. H.; Park, S. S. Heterogenization of Molecular Electrocatalytic Active Sites through Reticular Chemistry. *Adv. Mater.* **2023**, 35, No. 2203791.
- (2) Qiu, Z. M.; Li, Y.; Gao, Y. D.; Meng, Z. Y.; Sun, Y. Y.; Bai, Y.; Suen, N. T.; Chen, H. C.; Pi, Y. C.; Pang, H. 2D MOF-assisted Pyrolysis-displacement-alloying Synthesis of High-entropy Alloy Nanoparticles Library for Efficient Electrocatalytic Hydrogen Oxidation. *Angew. Chem., Int. Ed.* 2023, 62, No. e202306881.
- (3) Nam, K. W.; Park, S. S.; dos Reis, R.; Dravid, V. P.; Kim, H.; Mirkin, C. A.; Stoddart, J. F. Conductive 2D metal-organic framework for high-performance cathodes in aqueous rechargeable zinc batteries. *Nat. Commun.* **2019**, *10*, No. 4948.
- (4) Sheberla, D.; Bachman, J. C.; Elias, J. S.; Sun, C. J.; Shao-Horn, Y.; Dinca, M. Conductive MOF electrodes for stable supercapacitors with high areal capacitance. *Nat. Mater.* **2017**, *16*, 220–224.
- (5) Lu, H. Y.; Hu, J. S.; Zhang, K. Q.; Zhao, J. X.; Deng, S. Z.; Li, Y. J.; Xu, B. A.; Pang, H. Microfluidic-Assisted 3D Printing Zinc Powder Anode with 2D Conductive MOF/MXene Heterostructures for High-Stable Zinc-Organic Battery. *Adv. Mater.* **2023**, *36*, No. 2309753.
- (6) Campbell, M. G.; Liu, S. F.; Swager, T. M.; Dinca, M. Chemiresistive Sensor Arrays from Conductive 2D Metal-Organic Frameworks. J. Am. Chem. Soc. 2015, 137, 13780–13783.
- (7) Sun, L.; Liao, B. L.; Sheberla, D.; Kraemer, D.; Zhou, J. W.; Stach, E. A.; Zakharov, D.; Stavila, V.; Talin, A. A.; Ge, Y. C.; Allendorf, M. D.; Chen, G.; Léonard, F.; Dinca, M. A Microporous and Naturally Nanostructured Thermoelectric Metal-Organic Framework with Ultralow Thermal Conductivity. *Joule* 2017, 1, 168–177.
- (8) Xie, L. S.; Skorupskii, G.; Dinca, M. Electrically Conductive Metal-Organic Frameworks. *Chem. Rev.* **2020**, *120*, 8536–8580.
- (9) Debela, T. T.; Yang, M. C.; Hendon, C. H. Ligand-Mediated Hydrogenic Defects in Two-Dimensional Electrically Conductive Metal-Organic Frameworks. *J. Am. Chem. Soc.* **2023**, *145*, 11387–11391.
- (10) Wang, L.; Sarkar, A.; Grocke, G. L.; Laorenza, D. W.; Cheng, B. R.; Ritchhart, A.; Filatov, A. S.; Patel, S. N.; Gagliardi, L.; Anderson, J. S. Broad Electronic Modulation of Two-Dimensional Metal-Organic Frameworks over Four Distinct Redox States. *J. Am. Chem. Soc.* **2023**, 145, 8486–8497.
- (11) Hmadeh, M.; Lu, Z.; Liu, Z.; Gándara, F.; Furukawa, H.; Wan, S.; Augustyn, V.; Chang, R.; Liao, L.; Zhou, F.; Perre, E.; Ozolins, V.; Suenaga, K.; Duan, X. F.; Dunn, B.; Yamamto, Y.; Terasaki, O.; Yaghi, O. M. New Porous Crystals of Extended Metal-Catecholates. *Chem. Mater.* **2012**, *24*, 3511–3513.
- (12) Sheberla, D.; Sun, L.; Blood-Forsythe, M. A.; Er, S.; Wade, C. R.; Brozek, C. K.; Aspuru-Guzik, A.; Dinca, M. High Electrical Conductivity in Ni₃(2,3,6,7,10,11-hexaiminotriphenylene)₂, a Semiconducting Metal-Organic Graphene Analogue. *J. Am. Chem. Soc.* **2014**, *136*, 8859–8862.
- (13) Chen, T. Y.; Dou, J. H.; Yang, L. M.; Sun, C. Y.; Libretto, N. J.; Skorupskii, G.; Miller, J. T.; Dinca, M. Continuous Electrical Conductivity Variation in M_3 (Hexaiminotriphenylene)₂ (M = Co, Ni, Cu) MOF Alloys. *J. Am. Chem. Soc.* **2020**, *142*, 12367–12373.
- (14) Dong, R.; Han, P.; Arora, H.; Ballabio, M.; Karakus, M.; Zhang, Z.; Shekhar, C.; Adler, P.; St Petkov, P.; Erbe, A.; Mannsfeld, S. C. B.; Felser, C.; Heine, T.; Bonn, M.; Feng, X. L.; Canovas, E. Highmobility band-like charge transport in a semiconducting two-dimensional metal-organic framework. *Nat. Mater.* **2018**, *17*, 1027–1032.
- (15) Pal, T.; Kambe, T.; Kusamoto, T.; Foo, M. L.; Matsuoka, R.; Sakamoto, R.; Nishihara, H. Interfacial Synthesis of Electrically Conducting Palladium Bis(dithiolene) Complex Nanosheet. *Chem-PlusChem* **2015**, *80*, 1255–1258.
- (16) Cui, J. S.; Xu, Z. T. An electroactive porous network from covalent metal-dithiolene links. *Chem. Commun.* **2014**, *50*, 3986–3988.

- (17) Choi, J. Y.; Stodolka, M.; Kim, N.; Pham, H. T. B.; Check, B.; Park, J. 2D conjugated metal-organic framework as a proton-electron dual conductor. *Chem* **2023**, *9*, 143–153.
- (18) Huang, X.; Sheng, P.; Tu, Z. Y.; Zhang, F. J.; Wang, J. H.; Geng, H.; Zou, Y.; Di, C. A.; Yi, Y. P.; Sun, Y. M.; Xu, W.; Zhu, D. B. A two-dimensional π -conjugated coordination polymer with extremely high electrical conductivity and ambipolar transport behaviour. *Nat. Commun.* **2015**, *6*, No. 7408.
- (19) Dou, J. H.; Sun, L.; Ge, Y. C.; Li, W.; Hendon, C. H.; Li, J.; Gul, S.; Yano, J. K.; Stach, E. A.; Dinca, M. Signature of Metallic Behavior in the Metal-Organic Frameworks M₃(hexaiminobenzene)₂ (M = Ni, Cu). *J. Am. Chem. Soc.* **2017**, *139*, 13608–13611.
- (20) Dou, J. H.; Arguilla, M. Q.; Luo, Y.; Li, J.; Zhang, W. Z.; Sun, L.; Mancuso, J. L.; Yang, L. M.; Chen, T. Y.; Parent, L. R.; Skorupskii, G.; Libretto, N. J.; Sun, C. Y.; Yang, M. C.; Dip, P. V.; Brignole, E. J.; Miller, J. T.; Kong, J.; Hendon, C. H.; Sun, J. L.; Dinca, M. Atomically precise single-crystal structures of electrically conducting 2D metalorganic frameworks. *Nat. Mater.* **2021**, 20, 222–228.
- (21) Xing, G. L.; Liu, J. J.; Zhou, Y.; Fu, S.; Zheng, J. J.; Su, X.; Gao, X. F.; Terasaki, O.; Bonn, M.; Wang, H. I.; Chen, L. Conjugated Nonplanar Copper-Catecholate Conductive Metal-Organic Frameworks via Contorted Hexabenzocoronene Ligands for Electrical Conduction. J. Am. Chem. Soc. 2023, 145, 8979—8987.
- (22) Un, H. I.; Lu, Y.; Li, J. X.; Dong, R. H.; Feng, X. L.; Sirringhaus, H. Controlling Film Formation and Host-Guest Interactions to Enhance the Thermoelectric Properties of Nickel-Nitrogen-Based 2D Conjugated Coordination Polymers. *Adv. Mater.* **2024**, No. 2312325.
- (23) Liu, J. X.; Chen, Y. X.; Feng, X. L.; Dong, R. H. Conductive 2D Conjugated Metal-Organic Framework Thin Films: Synthesis and Functions for (Opto-)electronics. *Small Struct.* **2022**, *3*, No. 2100210.
- (24) (a) Choe, M.; Koo, J. Y.; Park, I.; Ohtsu, H.; Shim, J. H.; Choi, H. C.; Park, S. S. Chemical Vapor Deposition of Edge-on Oriented 2D Conductive Metal-Organic Framework Thin Films. *J. Am. Chem. Soc.* 2022, 144, 16726–16731. (b) Rubio-Giménez, V.; Arnauts, G.; Wang, M.; Oliveros Mata, E. S.; Huang, X.; Lan, T.; Tietze, M. L.; Kravchenko, D. E.; Smets, J.; Wauteraerts, N.; Khadiev, A.; Novikov, D. V.; Makarov, D.; Dong, R.; Ameloot, R. Chemical Vapor Deposition and High-Resolution Patterning of a Highly Conductive Two-Dimensional Coordination Polymer Film. *J. Am. Chem. Soc.* 2023, 145, 152–159.
- (25) Yao, M. S.; Lv, X. J.; Fu, Z. H.; Li, W. H.; Deng, W. H.; Wu, G. D.; Xu, G. Layer-by-Layer Assembled Conductive Metal-Organic Framework Nanofilms for Room-Temperature Chemiresistive Sensing. *Angew. Chem., Int. Ed.* **2017**, *56*, 16510–16514.
- (26) Lee, T.; Kim, J. O.; Park, C.; Kim, H.; Kim, M.; Park, H.; Kim, I.; Ko, J.; Pak, K.; Choi, S. Q.; Kim, I. D.; Park, S. Large-Area Synthesis of Ultrathin, Flexible, and Transparent Conductive Metal-Organic Framework Thin Films via a Microfluidic-Based Solution Shearing Process. *Adv. Mater.* **2022**, *34*, No. 2107696.
- (27) Marshall, C. R.; Timmel, E. E.; Staudhammer, S. A.; Brozek, C. K. Experimental evidence for a general model of modulated MOF nanoparticle growth. *Chem. Sci.* **2020**, *11*, 11539–11547.
- (28) Day, R. W.; Bediako, D. K.; Rezaee, M.; Parent, L. R.; Skorupskii, G.; Arguilla, M. Q.; Hendon, C. H.; Stassen, I.; Gianneschi, N. C.; Kim, P.; Dinca, M. Single Crystals of Electrically Conductive Two-Dimensional Metal-Organic Frameworks: Structural and Electrical Transport Properties. ACS Cent. Sci. 2019, 5, 1959—1964.
- (29) Luo, Y.; Wu, Y. H.; Braun, A.; Huang, C.; Li, X. Y.; Menon, C.; Chu, P. K. Defect Engineering To Tailor Metal Vacancies in 2D Conductive Metal-Organic Frameworks: An Example in Electrochemical Sensing. ACS Nano 2022, 16, 20820–20830.
- (30) Lu, Y.; Zhang, Y. Y.; Yang, C. Y.; Revuelta, S.; Qi, H. Y.; Huang, C. H.; Jin, W. L.; Li, Z. C.; Vega-Mayoral, V.; Liu, Y. N.; Huang, X.; Pohl, D.; Polozij, M.; Zhou, S. Q.; Cánovas, E.; Heine, T.; Fabiano, S.; Feng, X. L.; Dong, R. H. Precise tuning of interlayer electronic coupling in layered conductive metal-organic frameworks. *Nat. Commun.* 2022, 13, No. 7240.

- (31) Hendon, C. H.; Tiana, D.; Fontecave, M.; Sanchez, C.; D'arras, L.; Sassoye, C.; Rozes, L.; Mellot-Draznieks, C.; Walsh, A. Engineering the Optical Response of the Titanium-MIL-125 Metal-Organic Framework through Ligand Functionalization. *J. Am. Chem. Soc.* 2013, 135, 10942–10945.
- (32) Demuth, M. C.; Hendon, C. H. Linker Aromaticity Reduces Band Dispersion in 2D Conductive Metal-Organic Frameworks. *ACS Mater. Lett.* **2023**, *5*, 1476–1480.
- (33) Hoppe, B.; Hindricks, K. D. J.; Warwas, D. P.; Schulze, H. A.; Mohmeyer, A.; Pinkvos, T. J.; Zailskas, S.; Krey, M. R.; Belke, C.; König, S.; Fröba, M.; Haug, R. J.; Behrens, P. Graphene-like metalorganic frameworks: morphology control, optimization of thin film electrical conductivity and fast sensing applications. *CrystEngComm* **2018**, *20*, 6458–6471.
- (34) Spyrou, K.; Calvaresi, M.; Diamanti, E. A. K.; Tsoufis, T.; Gournis, D.; Rudolf, P.; Zerbetto, F. Graphite Oxide and Aromatic Amines: Size Matters. *Adv. Funct. Mater.* **2015**, *25*, 263–269.
- (35) Yang, H. B.; Miao, J. W.; Hung, S. F.; Chen, J. Z.; Tao, H. B.; Wang, X. Z.; Zhang, L. P.; Chen, R.; Gao, J. J.; Chen, H. M.; Dai, L. M.; Liu, B. Identification of catalytic sites for oxygen reduction and oxygen evolution in N-doped graphene materials: Development of highly efficient metal-free bifunctional electrocatalyst. *Sci. Adv.* **2016**, *2*, No. 1501122.
- (36) Mähringer, A.; Jakowetz, A. C.; Rotter, J. M.; Bohn, B. J.; Stolarczyk, J. K.; Feldman, J.; Bein, T.; Medina, D. D. Oriented Thin Films of Electroactive Triphenylene Catecholate-Based Two-Dimensional Metal-Organic Frameworks. *ACS Nano* **2019**, *13*, 6711–6719.
- (37) Wang, X. P.; Xi, S. B.; Huang, P. R.; Du, Y. H.; Zhong, H. Y.; Wang, Q.; Borgna, A.; Zhang, Y. W.; Wang, Z. B.; Wang, H.; Yu, Z. G.; Lee, W. S. V.; Xue, J. M. Pivotal role of reversible NiO₆ geometric conversion in oxygen evolution. *Nature* **2022**, *611*, 702–708.
- (38) Shimizu, K.-i.; Maeshima, H.; Yoshida, H.; Satsuma, A.; Hattori, T. Ligand field effect on the chemical shift in XANES spectra of Cu(II) compounds. *Phys. Chem. Chem. Phys.* **2001**, *3*, 862–866.
- (39) Frati, F.; Hunault, M. O. J. Y.; de Groot, F. M. F. Oxygen Kedge X-ray Absorption Spectra. *Chem. Rev.* **2020**, 120, 4056–4110.
- (40) Shadle, S. E.; Hedman, B.; Hodgson, K. O.; Solomon, E. I. Ligand K-Edge X-Ray-Absorption Spectroscopy as a Probe of Ligand-Metal Bonding Charge Donation and Covalency in Copper-Chloride Systems. *Inorg. Chem.* **1994**, 33, 4235–4244.
- (41) Song, X. Y.; Wang, X. Y.; Li, Y. S.; Zheng, C. Z.; Zhang, B. W.; Di, C. A.; Li, F.; Jin, C.; Mi, W. B.; Chen, L.; Hu, W. P. 2D Semiconducting Metal-Organic Framework Thin Films for Organic Spin Valves. *Angew. Chem., Int. Ed.* **2020**, *59*, 1118–1123.
- (42) Shimada, H.; Fukao, T.; Minami, H.; Ukai, M.; Fujii, K.; Yokoya, A.; Fukuda, Y.; Saitoh, Y. Nitrogen K-edge X-ray absorption near edge structure (XANES) spectra of purine-containing nucleotides in aqueous solution. *J. Chem. Phys.* **2014**, *141*, No. 055102.
- (43) Senarathna, M. C.; Li, H.; Perera, S. D.; Torres-Correas, J.; Diwakara, S. D.; Boardman, S. R.; Al-Kharji, N. M.; Liu, Y.; Smaldone, R. A. Highly Flexible Dielectric Films from Solution Processable Covalent Organic Frameworks. *Angew. Chem., Int. Ed.* **2023**, *62*, No. 202312617.
- (44) Burke, D. W.; Sun, C.; Castano, I.; Flanders, N. C.; Evans, A. M.; Vitaku, E.; McLeod, D. C.; Lambeth, R. H.; Chen, L. X.; Gianneschi, N. C.; Dichtel, W. R. Acid Exfoliation of Imine-linked Covalent Organic Frameworks Enables Solution Processing into Crystalline Thin Films. *Angew. Chem., Int. Ed.* **2020**, *59*, 5165–5171.
- (45) Ko, M.; Aykanat, A.; Smith, M. K.; Mirica, K. A. Drawing Sensors with Ball-Milled Blends of Metal-Organic Frameworks and Graphite. Sensors 2017, 17, No. 2192.
- (46) Smith, M. K.; Jensen, K. E.; Pivak, P. A.; Mirica, K. A. Direct Self-Assembly of Conductive Nanorods of Metal Organic Frameworks into Chemiresistive Devices on Shrinkable Polymer Films. *Chem. Mater.* **2016**, 28, 5264–5268.
- (47) Li, W. H.; Ding, K.; Tian, H. R.; Yao, M. S.; Nath, B.; Deng, W. H.; Wang, Y. B.; Xu, G. Conductive Metal-Organic Framework Nanowire Array Electrodes for High-Performance Solid-State Supercapacitors. *Adv. Funct. Mater.* **2017**, 27, No. 1702067.

- (48) Rubio-Giménez, V.; Galbiati, M.; Castells-Gil, J.; Almora-Barrios, N.; Navarro-Sánchez, J.; Escorcia-Ariza, G.; Mattera, M.; Arnold, T.; Rawle, J.; Tatay, S.; Coronado, E.; Martí-Gastaldo, C. Bottom-Up Fabrication of Semiconductive Metal-Organic Framework Ultrathin Films. *Adv. Mater.* **2018**, *30*, No. 1704291.
- (49) Cheng, P. H.; Chen, Q.; Liu, H. Y.; Liu, X. R. Exploration of conjugated π -bridge units in N_iN -bis(4-methoxyphenyl)naphthalen-2-amine derivative-based hole transporting materials for perovskite solar cell applications: a DFT and experimental investigation. *RSC Adv.* **2021**, *12*, 1011–1020.